arXiv:nucl-th/9910032v1 12 Oct 1999

Configuration mixing of mean-field wave-functions projected on angular momentum and particle number; application to ^{24}Mg

A. Valor, P.-H. Heenen

Service de Physique Nucléaire Théorique et de Physique Mathématique, U.L.B - C.P. 229, B 1050 Brussels, Belgium

P. Bonche

SPhT CEA Saclay, F 91191 Gif sur Yvette Cedex, France

Abstract

We present in this paper the general framework of a method which permits to restore the rotational and particle number symmetries of wave functions obtained in Skyrme HF+BCS calculations. This restoration is nothing but a projection of mean-field intrinsic wave functions onto good particle number and good angular momentum. The method allows also to *mix* projected wave functions. Such a configuration mixing is discussed for sets of HF+BCS intrinsic states generated in constrained calculations with suitable collective variables. This procedure gives collective states which are eigenstates of the particle number and the angular momentum operators and between which transition probabilities are calculated. An application to ^{24}Mg is presented, with mean-field wave functions generated by axial quadrupole constraints. Theoretical spectra and transition probabilities are compared to the experiment.

PACS numbers: 21.10.Ky 21.30.-n 21.60.Jz 27.30+t

---

1 Introduction

The cranking method is widely used in nuclear spectroscopy to describe high spin states. Applications based on effective nuclear interactions have been particularly successful in the description of super-deformed rotational bands in several regions of the mass table [1–5]. In the cranking method, a rotational band is generated by the rotation of a deformed intrinsic state. Since cranking states are not eigenstates of angular momentum, it is not straightforward to determine transition rates in nuclei which are not very well deformed. To overcome this difficulty, approximations [6–8] have been developed for transitions within a band. However, they are only valid when the structure of the nuclear states are not affected by rotation, i.e. for rigid nuclei.

Another limitation of the cranking model occurs in nuclei soft with respect to the variation of a collective variable. In this case, one expects that the interference of the zero-point vibrational mode with the rotational motion will lead to variations in the nuclear structure along the yrast line.

There have been several attempts in the past to introduce phenomenological corrections taking into account rotational and vibrational corrections to the mean-field energy (see for instance [9–11]). It is the aim of the present paper to introduce a method in which rotations and vibrations are taken into account simultaneously in a more general and consistent way.

The starting point of our approach is a set of many-body wave functions generated by constrained Skyrme HF+BCS calculations. The discretization of these wave functions on a 3-dimensional Cartesian mesh enables to describe very general shapes of the nuclear density and to easily write the effect of a spatial rotation on the mean-field wave functions. This property permits to restore symmetries with respect to angular momentum and to the proton and neutron particle numbers in a systematic way.

It is not the first time that symmetries are restored on mean-field wave functions. Several methods have been developed for schematic nuclear interactions and a limited number of active valence nucleons (for recent references, see [12,13]). Methods based on effective interactions have been limited to either angular momentum [14–16] or particle number projection with mixing of configurations by the generator coordinate method (GCM) [17]. The present work generalizes this last work by the inclusion of a projection on angular momentum.

We present below the general framework of our method together with a test on a light nucleus for which extensive calculations can be performed. In the first part, we show how to implement the projection on $\vec{J}$, N and Z simultaneously and to determine the contractions needed to calculate the matrix elements between two different many-body HFB vacua. The specificities of mesh calculations require to take explicitly into account the fact that the single-particle bases are not complete and lead to formulae rather different from some similar works [18,13]. In the second part of this work, we present an application to the ^{24}Mg nucleus for which the properties of several effective interactions are tested.

2 Angular momentum and particle number projections

2.1 Principle of the method

The starting point of our method is a set of wave functions $|\Phi_\alpha\rangle$ generated by mean-field calculations with a constraint on a collective coordinate α. Wave functions with good angular momentum and particle numbers are obtained by restorations of symmetry on $|\Phi_\alpha\rangle$:

$$|\Phi, JM\alpha\rangle = \frac{1}{\mathcal{N}} \sum_K g_K \hat{P}^J_{MK} \hat{P}^Z \hat{P}^N |\Phi_\alpha\rangle \quad , \tag{1}$$

where $\mathcal{N}$ is a normalization factor, and the operators $\hat{P}$ are projectors.

A configuration mixing on the collective variable α is then performed for each angular momentum:

$$|\Psi, JM\rangle = \sum_\alpha f^{JM}_\alpha |\Phi, JM\alpha\rangle \quad . \tag{2}$$

The weight functions f^{JM}_α are found by requiring that the expectation value of the energy:

$$E^{JM} = \frac{\langle \Psi, JM|\hat{H}|\Psi, JM\rangle}{\langle \Psi, JM|\Psi, JM\rangle} \quad , \tag{3}$$

is stationary with respect to an arbitrary variation δf^{JM}_α. This prescription leads to the discretized Hill-Wheeler equation [19]:

$$\sum_\alpha (\mathcal{H}^{JM}_{\alpha,\alpha'} - E^{JM}_k \mathcal{I}^{JM}_{\alpha,\alpha'}) f^{JM,k}_{\alpha'} = 0 \quad , \tag{4}$$

in which the Hamiltonian kernel $\mathcal{H}^{JM}$ and the overlap kernel $\mathcal{I}^{JM}$ are defined as

$$\mathcal{H}^{JM}_{\alpha,\alpha'} = \langle \Phi JM\alpha|\hat{H}|\Phi JM\alpha'\rangle, \quad \mathcal{I}^{JM}_{\alpha,\alpha'} = \langle \Phi JM\alpha|\Phi JM\alpha'\rangle \quad . \tag{5}$$

Since the Hamiltonian is rotationally invariant (we will come back to the problem of the density dependence of the interaction in section 2.8) and conserves the number of particles, one has to restore the symmetries on only one of the two wave functions entering in each matrix element like eq. (5). The kernels are obtained by integration on three Euler angles and two gauge angles of the matrix elements between rotated wave functions.

Besides these kernels, we will calculate transition probabilities between different eigenstates of the Hill-Wheeler equation. This requires the calculation of the matrix elements of a tensor of order L, $\hat{T}^M_L$, between projected states.

Such a secular problem based on the configuration mixing defined by eq. 2 amounts to a variation after projection in a many-body Hilbert space built on a limited set of states obtained for different values of the collective variables α's.

2.2 Determination of the contractions

The matrix elements (eq. 5) are calculated in two steps. They are first determined for a given rotation and for given gauge angles. Then they are integrated over the Euler and gauge angles.

To compute the kernels, we make use of the Balian-Brézin theorem [20] which expresses them in terms of contractions of creation and/or annihilation single-particle operators.

To simplify the presentation, the spatial rotation is applied on the left wave function, whereas the particle number rotation is applied on the right one. The wave functions after rotation are denoted by $|L\rangle$ and $|R\rangle$ and the associated quasiparticle annihilation operators by l_μ, r_μ respectively, with $\mu = 1, \ldots, N$. The number N is the total number of HF states included in the mean-field calculations.

The quasiparticle operators are obtained by the diagonalization of the Bogoliubov equations on a single-particle basis. When the equations are discretised on a 3D mesh, a convenient basis is provided by the eigenstates of the HF Hamiltonian. Since only a limited number of single-particle HF states are determined, the left and right bases are different. The particle annihilation and creation operators of the left and right particle bases will be denoted (a, a^+) and (b, b^+) respectively. They are related by a unitary transformation:

$$a_\mu = \sum_\nu R_{\mu,\nu} b_\nu \quad . \tag{6}$$

The quasiparticle operators l_μ and r_μ are expressed as a function of the left and right single-particle bases by Bogoliubov transformations [8]:

$$\begin{pmatrix} \mathbf{l} \\ \mathbf{l}^+ \end{pmatrix} = \begin{pmatrix} U_l^{B\dagger} & V_l^{B\dagger} \\ V_l^{BT} & U_l^{BT} \end{pmatrix} \begin{pmatrix} \mathbf{a} \\ \mathbf{a}^+ \end{pmatrix} \equiv W^\dagger \begin{pmatrix} \mathbf{a} \\ \mathbf{a}^+ \end{pmatrix} \quad ; \tag{7}$$

where the matrices U_l^B and V_l^B have dimensions N x N. The expressions for the right quasi-particles are similar.

Using the same notations as in [21], we define the two vectors

$$\lambda = \begin{pmatrix} \mathbf{l} \\ \mathbf{l}^+ \end{pmatrix} \quad , \qquad \rho = \begin{pmatrix} \mathbf{r} \\ \mathbf{r}^+ \end{pmatrix} \quad , \tag{8}$$

in terms of which any two-body operator $\hat{O}$ can be expressed.

The quasiparticle bases are related by a linear transformation $\hat{T}$. Taking into account that the matrix R linking the HF single-particle bases does not mix creation and annihilation operators, one obtains:

$$\lambda = \hat{T}\rho, \quad \hat{T} = \begin{pmatrix} (D^{-1})^* & -E \\ -E^* & D^{-1} \end{pmatrix}, \tag{9}$$

where,

$$D = (U_l^{B^T} R U_r^{B*} + V_l^{B^T} R V_r^{B*})^{-1}, \qquad E = -(U_l^{B+} R V_r^{B*} + V_l^{B+} R U_r^{B*}), \tag{10}$$

Balian and Brézin [20] have established the relation between $\hat{T}$ and the contractions $\langle \lambda\rho \rangle$, $\langle \rho\rho \rangle$ and $\langle \lambda\lambda \rangle$:

$$\langle \lambda\lambda \rangle = \begin{pmatrix} \langle \mathbf{ll} \rangle & 1 \\ 0 & 0 \end{pmatrix} = \begin{pmatrix} ED & 1 \\ 0 & 0 \end{pmatrix} \quad , \tag{11}$$

$$\langle \rho\rho \rangle = \begin{pmatrix} 0 & 1 \\ 0 & \langle \mathbf{r}^+\mathbf{r}^+ \rangle \end{pmatrix} = \begin{pmatrix} 0 & 1 \\ 0 & DE^* \end{pmatrix} \quad , \tag{12}$$

$$\langle \lambda\rho \rangle = \begin{pmatrix} 0 & \langle \mathbf{l}\mathbf{r}^+ \rangle \\ 0 & 0 \end{pmatrix} = \begin{pmatrix} 0 & D^T \\ 0 & 0 \end{pmatrix} \quad . \tag{13}$$

In addition, they have derived a formula for the modulus of the overlap between left and right many-body wave functions:

$$\langle L|R \rangle = \pm(\det D^{-1})^{1/2} \tag{14}$$

One obtains the contractions in the particle bases:

$$\begin{aligned}\langle \mathbf{a}^+\mathbf{b}\rangle &= V_l^B D^T V_r^{B+} \quad , \\ \langle \mathbf{a}^+\mathbf{a}^+\rangle &= V_l^B U_l^{B+} + V_l^B E D V_l^{B T} \quad , \\ \langle \mathbf{b}\mathbf{b}\rangle &= U_r^B V_r^{B+} + V_r^{B*} D E^* V_r^{B+} \quad .\end{aligned} \tag{15}$$

2.3 Symmetry restrictions

The formulae derived in section 2.2 are general. In the present application, we impose several symmetry restrictions on the mean-field wave functions. These restrictions which we develop below do not limit the formalism, they are only intended to simplify the equations for our test case. They can be released, if need be, at the only cost of additional computational time.

First, the total wave function is symmetric with respect to reflections across the $x = 0$, $y = 0$ and $z = 0$ planes and time-reversal invariant. With this symmetry restriction to ellipsoidal configurations, the single-particle wave functions are described by 4-dimensional vectors [22],

$$\begin{pmatrix} w_{1,\mu} \\ w_{2,\mu} \\ w_{3,\mu} \\ w_{4,\mu} \end{pmatrix} = \begin{pmatrix} Re\ \Phi_\mu(\mathbf{r},+,+,+p) \\ Im\ \Phi_\mu(\mathbf{r},-,-,+p) \\ Re\ \Phi_\mu(\mathbf{r},-,+,-p) \\ Im\ \Phi_\mu(\mathbf{r},+,-,-p) \end{pmatrix} \quad , \tag{16}$$

where the components describe, respectively, the real and imaginary spin up and down parts of the single-particle wave functions. The total parity is given by p. Each of the components has a well defined symmetry with respect to reflections across the three planes $x = 0$, $y = 0$ and $z = 0$ (see Ref. [21], appendix C). In a mesh calculation, the space is limited to a box beyond which all the wave functions are set to zero. With these symmetries, all the integrations can be limited to an octant of the box.

A second restriction is that the intrinsic wave functions have been generated by constraints on the axial quadrupole moment only, the z-axis being the symmetry axis of the nucleus. To restore angular momentum requires then only to rotate the mean-field wave function by an angle β around the y-axis. The coordinates (x_0, y_0, z_0) become after rotation:

$$\begin{aligned} x_1 &= z_0 \sin(\beta) + x_0 \cos(\beta) \quad , \\ y_1 &= y_0 \quad , \\ z_1 &= z_0 \cos(\beta) - x_0 \sin(\beta) \quad , \end{aligned} \tag{17}$$

and the four components of a wave function rotate according to:

$$\begin{aligned}
p_{1,\mu}(\mathbf{r}_1) &= w_{1,\mu}(\mathbf{r}_0)\cos(\beta/2) - w_{3,\mu}(\mathbf{r}_0)\sin(\beta/2) \\
p_{2,\mu}(\mathbf{r}_1) &= w_{2,\mu}(\mathbf{r}_0)\cos(\beta/2) - w_{4,\mu}(\mathbf{r}_0)\sin(\beta/2) \\
p_{3,\mu}(\mathbf{r}_1) &= w_{3,\mu}(\mathbf{r}_0)\cos(\beta/2) + w_{1,\mu}(\mathbf{r}_0)\sin(\beta/2) \\
p_{4,\mu}(\mathbf{r}_1) &= w_{4,\mu}(\mathbf{r}_0)\cos(\beta/2) + w_{2,\mu}(\mathbf{r}_0)\sin(\beta/2) \quad .
\end{aligned} \tag{18}$$

These equations show that while the total parity p is preserved by a rotation, the specific symmetries of the four components with respect to the $x = 0$ and $z = 0$ planes are lost. In the same way, signature as defined in ref [22] is not conserved. An immediate consequence of this loss of symmetry is that matrix elements between rotated and non rotated wave functions must be calculated in half of a box. The real and imaginary parts of the rotated wave function have different symmetries with respect to the $y = 0$ plane and the overlap between rotated and non rotated individual wave functions are real.

Furthermore, the points (x_1, y_1, z_1) do not coincide after rotation with mesh points. The values of the rotated wave functions on the mesh points are reevaluated using the analytical forms of functions defined on a mesh given in ref [23].

The relation between rotated (left) and non rotated (right) operators is given by:

$$a_\mu = \sum_{\nu>0}\{R_{\mu,\nu}b_\nu + R_{\mu,\overline{\nu}}b_{\overline{\nu}}\} \quad , \qquad a_{\overline{\mu}} = \sum_{\nu>0}\{R_{\overline{\mu},\nu}b_\nu + R_{\overline{\mu},\overline{\nu}}b_{\overline{\nu}}\} \quad , \tag{19}$$

where the state $|\overline{\mu}\rangle$ denotes the time-reversed partner of state $|\mu\rangle$ and the matrix R is given by the overlap between left and right states. Using the properties of the time reversal operator, one can show the following relations between the overlaps:

$$R_{\overline{\mu},\nu} = -R_{\mu,\overline{\nu}} \quad , \qquad R_{\overline{\mu},\overline{\nu}} = R_{\mu,\nu} \quad . \tag{20}$$

The matrix R does not separate into blocks corresponding to the different combinations of parity and signature as in our previous study [17].

2.4 Restriction to BCS transformations

One can still simplify the expressions for contractions derived in sub-section 2.2 for the general Bogoliubov transformations to BCS transformations. This limitation should not be too bad for even nuclei close to the stability line, as ^{24}Mg, for which pairing correlations do not couple significantly bound and continuum states.

The state $|R\rangle$ is obtained from the original intrinsic state by multiplying by a phase $e^{2i\phi}$ the occupation numbers in the original BCS (or HFB) transformation

$$|R\rangle \equiv |R(\phi)\rangle \Longleftrightarrow \begin{cases} r_\mu = u_{r\mu} b_\mu - v_{r\mu} e^{i2\phi} b^+_{\overline{\mu}} \\ r_{\overline{\mu}} = u_{r\mu} b_{\overline{\mu}} + v_{r\mu} e^{i2\phi} b^+_{\mu} \end{cases} ,$$

with $u_{r\mu}$, $v_{r\mu}$ real and positive, and $u_{r\overline{\mu}} = u_{r\mu}$, $v_{r\overline{\mu}} = -v_{r\mu}$.

In the BCS case the matrices U^B_l, V^B_l, U^B_r, V^B_r take the form

$$U^B_l \equiv U_l \ ; \quad V^B_l \equiv -\sigma V_l \ ; \quad U_l = \begin{pmatrix} u_l & 0 \\ 0 & u_l \end{pmatrix} \ ; \quad V_l = \begin{pmatrix} v_l & 0 \\ 0 & v_l \end{pmatrix} \ ; \tag{21}$$

$$U^B_r \equiv U_r \ ; \quad V^B_r \equiv -\sigma V_r e^{-i2\phi} \ ; \quad U_r = \begin{pmatrix} u_r & 0 \\ 0 & u_r \end{pmatrix} \ ; \quad V_r = \begin{pmatrix} v_r & 0 \\ 0 & v_r \end{pmatrix} \ ; \tag{22}$$

The matrices u_l, v_l, u_r, v_r, are real, diagonal and of dimension N/2 x N/2. The matrix σ is defined as

$$\sigma = \begin{pmatrix} 0 & -1 \\ 1 & 0 \end{pmatrix} \quad . \tag{23}$$

Thanks to the symmetry properties given by equation (20), the matrices D and E introduced in subsection 2.2 have the same block structure as matrix R. These same symmetries allow the relation $\sigma^T R \sigma = R$. We can thus write the contractions, as well as matrices D, E, in a simpler way. We have:

$$\begin{aligned} \langle \mathbf{a}^+ \mathbf{b} \rangle &= V_l D^T V_r e^{2i\phi} \ ; & D &= V_l R V_r e^{2i\phi} + U_l R U_r \ ; \\ \langle \mathbf{a}^+ \mathbf{a}^+ \rangle &= -\sigma (V_l U_l - V_l \tilde{E} D V_l) \ ; & E &= \sigma \tilde{E} \ ; \\ \langle \mathbf{b} \mathbf{b} \rangle &= \sigma (U_r V_r + V_r D \tilde{E}^* V_r e^{2i\phi}) e^{2i\phi} \ ; & \tilde{E} &= U_l R V_r e^{2i\phi} - V_l R U_r \ . \end{aligned}$$

2.5 Elimination of non occupied states

In the derivation shown in the above section, it is assumed that left and right bases are either complete or truncated in such a way that they span the same space. As discussed in ref [21], this property is not valid when orbitals are discretized on a three dimensional mesh. This problem can be solved by taking into account that the missing part of the expansion of the left states on the right basis includes empty states that do not affect the structure of the nucleus.

These states are defined by the condition $v_\mu = 0$ and contribute neither to the overlap nor to the contractions. Since the structure of the matrices is different than in ref [21], we give now the formulae corresponding to the present case.

Let us introduce:

$$V_l = \begin{pmatrix} \overline{V}_l & 0 \\ 0 & 0 \end{pmatrix} \quad ; \quad U_l = \begin{pmatrix} \overline{U}_l & 0 \\ 0 & 1 \end{pmatrix} \quad ; \tag{24}$$

and split the unitary matrix R in the form

$$R = \begin{pmatrix} \mathcal{R} & \mathcal{I} \\ \mathcal{T} & \mathcal{U} \end{pmatrix} \quad . \tag{25}$$

With these notations, the contractions can be written as:

$$\langle \mathbf{a}^+ \mathbf{b} \rangle = \begin{pmatrix} \overline{V}_l \mathcal{D}^T \overline{V}_r e^{2i\phi} & 0 \\ 0 & 0 \end{pmatrix} \quad ; \tag{26}$$

$$\langle \mathbf{b}\mathbf{b} \rangle = \sigma \begin{pmatrix} \overline{U}_r \overline{V}_r + \overline{V}_r \mathcal{D} \mathcal{E}_r \overline{V}_r & 0 \\ 0 & 0 \end{pmatrix} \quad ; \tag{27}$$

$$\langle \mathbf{a}^+ \mathbf{a}^+ \rangle = -\sigma \begin{pmatrix} \overline{V}_l \overline{U}_l - \overline{V}_l \mathcal{E}_l \mathcal{D} \overline{V}_l & 0 \\ 0 & 0 \end{pmatrix} \quad . \tag{28}$$

The matrices $\mathcal{D}$, $\mathcal{E}_r$ and $\mathcal{E}_l$ are defined by:

$$\mathcal{D} = \left(\overline{U}_l (\mathcal{R}^+)^{-1} \overline{U}_r + \overline{V}_l \mathcal{R} \overline{V}_r e^{2i\phi} \right)^{-1} \quad ; \tag{29}$$

$$\mathcal{E}_r = \overline{U}_l (\mathcal{R}^+)^{-1} \overline{V}_r - \overline{V}_l \mathcal{R} \overline{U}_r e^{2i\phi} \quad ; \tag{30}$$

$$\mathcal{E}_l = \overline{U}_l \mathcal{R} \overline{V}_r e^{2i\phi} - \overline{V}_l (\mathcal{R}^+)^{-1} \overline{U}_r \quad . \tag{31}$$

2.6 Determination of the overlap

2.6.1 Modulus

Equation (14) gives the overlaps up to a sign. Several methods have been developed to calculate the global phase of the overlap. We show in the next section which procedure we have implemented. In this section, we give the explicit formulae for the modulus of the overlap. We have:

$$D^{-1} = U_l R U_r + V_l R V_r e^{2i\phi} \quad , \tag{32}$$

so that:

$$\begin{aligned}\langle L|R\rangle &= \pm(\det(D^{-1}))^{1/2} \\ &= \pm\left(\det\begin{pmatrix}\overline{U}_l\mathcal{R}\overline{U}_r + \overline{V}_l\mathcal{R}\overline{V}_r e^{2i\phi} & \overline{U}_l\mathcal{I} \\ \mathcal{T}\overline{U}_r & \mathcal{U}\end{pmatrix}\right)^{1/2} \quad .\end{aligned} \tag{33}$$

It is easy, although tedious, to demonstrate that the matrix D,

$$D = \begin{pmatrix}\mathcal{D}; & \mathcal{D}\overline{U}_l(\mathcal{R}^+)^{-1}\mathcal{T}^+ \\ \mathcal{I}^+(\mathcal{R}^+)^{-1}\overline{U}_r\mathcal{D}; & \mathcal{U}^{-1} + \mathcal{I}^+(\mathcal{R}^+)^{-1}\overline{U}_r\mathcal{D}\overline{U}_l(\mathcal{R}^+)^{-1}\mathcal{T}^+\end{pmatrix} , \tag{34}$$

where $\mathcal{D}$ is given by eq. 29, can be expressed as the product of four matrices [24]:

$$D = \begin{pmatrix}\overline{U}_r^{-1} & 0 \\ 0 & 1\end{pmatrix}\begin{pmatrix}\mathcal{R}^+ & \mathcal{T}^+ \\ \mathcal{I}^+ & \mathcal{U}^+\end{pmatrix}\begin{pmatrix}\alpha_r^{-1} & 0 \\ 0 & 1\end{pmatrix}\begin{pmatrix}1 & -\beta_r \\ 0 & 1\end{pmatrix} \quad , \tag{35}$$

with:

$$\begin{aligned}\alpha_r &= \overline{U}_l + \overline{V}_l\mathcal{R}\overline{V}_r\overline{U}_r^{-1}\mathcal{R}^+ e^{2i\phi} , \\ \beta_r &= \overline{V}_l\mathcal{R}\overline{V}_r\overline{U}_r^{-1}\mathcal{T}^+ e^{2i\phi} ;\end{aligned} \tag{36}$$

so that

$$\begin{aligned}\det D &= \det(\overline{U}_r^{-1})\det(R^+)\det(\alpha_r^{-1}) \\ &= \det(\overline{U}_r^{-1}\alpha_r^{-1}) \\ &= \det\left[((\mathcal{R}^+)^{-1})\right]\det(\mathcal{D}) ,\end{aligned} \tag{37}$$

where we have taken into account that the determinant of the unitary matrix R equals 1. We finally obtain:

$$\langle L|R\rangle(\phi) = \pm \left(\frac{\det \mathcal{R}}{\det \mathcal{D}} \right)^{1/2} \quad . \tag{38}$$

2.6.2 Phase

For any space rotation angle β, the overlap between two mean-field wave functions is positive for $\phi_n = 0$ and $\phi_p = 0$. We need to follow the evolution of the phase of the overlap along the integration paths on ϕ_n and ϕ_p. One has:

$$\langle L|R\rangle(\phi) = \sqrt{(\mathrm{Re}[\langle L|R\rangle(\phi)])^2 + (\mathrm{Im}[\langle L|R\rangle(\phi)])^2} e^{i\Omega(\phi)} \; . \tag{39}$$

We can rewrite the global phase Ω as:

$$\Omega(\phi) = \mathrm{Im} \ln(\langle L|R\rangle(\phi)) = \Phi(\phi) + n(\phi)\pi \; , \tag{40}$$

where Φ, which can be defined as:

$$\Phi(\phi) = \arctan(\mathrm{Im}[\langle L|R\rangle(\phi)]/\mathrm{Re}[\langle L|R\rangle(\phi)]) \quad , \tag{41}$$

is limited to the interval $[-\pi/2 \; , \; \pi/2]$. The integer number n remains to be determined. The total phase and its derivative are given by:

$$\frac{d\Omega(\phi)}{d\phi} = \mathrm{Re} \left\{ \frac{\langle L|\hat{N}|R\rangle(\phi)}{\langle L|R\rangle(\phi)} \right\} \quad . \tag{42}$$

It can also be calculated directly from the matrix element of the particle number operator:

$$\begin{aligned} \frac{\langle L|\hat{N}|R\rangle(\phi)}{\langle L|R\rangle(\phi)} &= \sum_{\mu>0} \langle a_\mu^+ a_\mu \rangle_\phi + \langle a_{\overline{\mu}}^+ a_{\overline{\mu}} \rangle_\phi \; , \\ &= 2 \sum_{\mu,\mu'>0} \{ R_{\mu\mu'} \langle a_\mu^+ b_{\mu'} \rangle_\phi + R_{\mu\overline{\mu}'} \langle a_\mu^+ b_{\overline{\mu}'} \rangle_\phi \} \; , \\ &= 2 \sum_{\mu,\mu'>0} \{ \mathcal{R}_{\mu\mu'} (\overline{V}_l \mathcal{D}^T \overline{V}_r)_{\mu\mu'} \mathrm{e}^{2i\phi} + \mathcal{R}_{\mu\overline{\mu}'} (\overline{V}_l \mathcal{D}^T \overline{V}_r)_{\mu\overline{\mu}'} \mathrm{e}^{2i\phi} \} \; , \end{aligned} \tag{43}$$

where we have used the symmetry properties discussed in the previous section and eq. (26) for the contractions $\langle \mathbf{a}^+ \mathbf{b} \rangle$.

Using this formula, we determine the phase of the overlap with a method similar to the one developed in ref [25,13]. Starting from $\phi = 0$, for which n(ϕ)=0, the value of the phase at neighboring angles is determined by:

$$\Omega(\phi + \delta\phi) \backsimeq \Omega(\phi) + \frac{\pi}{2L}\left[\frac{\delta}{\delta\phi}\Omega(\phi) + \frac{\delta}{\delta\phi}\Omega(\phi + \delta\phi)\right] , \tag{44}$$

where we have taken into account that the interval of integration has a length π and is divided into L segments of equal dimension $\delta\phi = \pi/L$. From the comparison between $\Omega(\phi + \delta\phi)$ calculated from (44) and $\Phi(\phi + \delta\phi)$ obtained from (41), one determines n(ϕ), provided the mesh is dense enough ($\delta\phi$ small enough).

2.7 Calculation of multipole moments and transition probabilities

The determination of transition probabilities requires the calculation of the matrix element of a tensor of order L, $\hat{T}_L^M$, between eigenstates of the angular momentum operator.

An eigenstate of the angular momentum operator, with eigenvalue J, is obtained by projecting the mean-field wave function $|\Phi\rangle$:

$$|\Phi, JM\rangle = \frac{\sum_K g_K \hat{P}^J_{MK}|\Phi\rangle}{\{\sum_K |g_K|^2 \langle\Phi|\hat{P}^J_{KK}|\Phi\rangle\}^{1/2}} , \tag{45}$$

where the projector is given by [8]:

$$\hat{P}^J_{MK} = \frac{2J+1}{8\pi^2}\int d\Omega D^{J*}_{MK}(\Omega)\hat{R}(\Omega) , \tag{46}$$

with $\Omega \equiv (\alpha, \beta, \gamma)$ the Euler angles and $\hat{R}(\Omega) \equiv e^{i\alpha\hat{J}_z}e^{i\beta\hat{J}_y}e^{i\gamma\hat{J}_z}$.

Only the K=0 term of this expression is present with the symmetry restrictions that we have imposed. Then:

$$\langle JM, \Phi|\hat{T}^0_L|J'M', \Phi'\rangle = \frac{\langle\Phi|\hat{P}^J_{0M}\hat{T}^0_L\hat{P}^{J'}_{M'0}|\Phi'\rangle}{\{\langle\Phi|\hat{P}^J_{00}|\Phi\rangle\langle\Phi'|\hat{P}^{J'}_{00}|\Phi'\rangle\}^{1/2}} , \tag{47}$$

where we have used the properties $(\hat{P}^J_{MK})^+ = \hat{P}^J_{KM}$ and $\hat{P}^J_{MK}\hat{P}^{J'}_{M'K'} = \delta_{JJ'}\delta_{KM'}\hat{P}^J_{MK'}$ of the angular momentum projector operator [26].

We have

$$\langle JM,\Phi|\hat{T}^0_L|J^{'}M^{'},\Phi^{'}\rangle = \frac{\sqrt{(2J+1)(2J'+1)}}{8\pi^2}$$

$$\frac{\int d\Omega d\Omega' D^{J*}_{0M}(\Omega) D^{J'*}_{M'0}(\Omega')\langle\Phi|\hat{R}(\Omega)\hat{T}^0_L\hat{R}(\Omega')|\Phi'\rangle}{\left\{\left[\int d\Omega D^{J*}_{00}(\Omega)\langle\Phi|\hat{R}(\Omega)|\Phi\rangle\right]\left[\int d\Omega' D^{J'*}_{00}(\Omega')\langle\Phi'|\hat{R}(\Omega')|\Phi'\rangle\right]\right\}^{1/2}}\ . \tag{48}$$

The axial symmetry reduces the integration interval to $[0,\pi/2]$. Moreover, thanks to the transformation of the wave functions under rotation (see eq. 18), the matrix element $\langle\Phi|\hat{T}^0_L \mathrm{e}^{i\beta\hat{J}_y}|\Phi'\rangle$ is real and is the same for rotations of angles β and $-\beta$. In the case of axial symmetry, the final expression takes then the form:

$$\langle JM,\Phi|\hat{T}^0_L|J'M',\Phi'\rangle = \frac{1}{2}\sqrt{\frac{2J'+1}{2J+1}}\langle J'ML0|JM\rangle\langle J'0L0|J0\rangle\delta_{MM'}$$

$$\frac{\left[\int \sin\beta d\beta d^J_{00}(\beta)\langle\Phi|\mathrm{e}^{i\beta\hat{J}_y}\hat{T}^0_L|\Phi'\rangle + \int \sin\beta d\beta d^{J'}_{00}(\beta)\langle\Phi'|\mathrm{e}^{i\beta\hat{J}_y}\hat{T}^0_L|\Phi\rangle\right]}{\left[\int \sin\beta d\beta d^J_{00}(\beta)\langle\Phi|\mathrm{e}^{i\beta\hat{J}_y}|\Phi\rangle\right]^{1/2}\left[\int \sin\beta' d\beta' d^{J'}_{00}(\beta')\langle\Phi'|\mathrm{e}^{i\beta'\hat{J}_y}|\Phi'\rangle\right]^{1/2}}\ . \tag{49}$$

In the case of electric quadrupole transitions, the diagonal matrix element takes the form:

$$\langle JM=0,\Phi|\hat{Q}_{20}|JM=0,\Phi\rangle = \langle J020|J0\rangle^2 \frac{\left[\int \sin\beta d\beta d^J_{00}(\beta)\langle\Phi|\mathrm{e}^{i\beta\hat{J}_y}\hat{Q}_{20}|\Phi\rangle\right]}{\left[\int \sin\beta d\beta d^J_{00}(\beta)\langle\Phi|\mathrm{e}^{i\beta\hat{J}_y}|\Phi\rangle\right]}$$

$$= \frac{(J+1)J}{(2J+3)(2J-1)}\frac{\left[\int \sin\beta d\beta d^J_{00}(\beta)\langle\Phi|\mathrm{e}^{i\beta\hat{J}_y}\hat{Q}_{20}|\Phi\rangle\right]}{\left[\int \sin\beta d\beta d^J_{00}(\beta)\langle\Phi|\mathrm{e}^{i\beta\hat{J}_y}|\Phi\rangle\right]} \tag{50}$$

The transition matrix elements between GCM states are obtained as the weighted sums of the contributions of the different basis states.

We finally obtain for the reduced transition probability between the initial, l$_i$-th GCM collective state of spin I$_i$, to the final, l$_f$-th GCM collective state of spin I$_f$:

$$B(EL, I_i^{(l_i)} \to I_f^{(l_f)}) = \frac{e^2}{4}\langle I_i0L0|I_f0\rangle^2$$

$$\frac{\left[\int\int dada' f^{(I_f^+,l_f)*}(a) f^{(I_i^+,l_i)}(a')\int dcos\beta d^{I_f}_{00}(\beta)\langle\Phi(a)|\mathrm{e}^{i\beta\hat{J}_y}\mathcal{M}_{L0}|\Phi'(a')\rangle + (I_f^+,l_f\leftrightarrow I_i^+,l_i)\right]^2}{\left[\int\int dada' f^{(I_f^+,l_f)*}(a) f^{(I_f^+,l_f)}(a')\int dcos\beta d^{I_f}_{00}(\beta)\langle\Phi(a)|\mathrm{e}^{i\beta\hat{J}_y}|\Phi'(a')\rangle\right]\left[(I_f^+,l_f\leftrightarrow I_i^+,l_i)\right]}, \tag{51}$$

with $\mathcal{M}_{L0} = r^2 Y_{L0}(\theta,\phi)$.

2.8 Density dependence of the effective interactions

The density dependent term of the interaction must be generalized to calculate non diagonal matrix elements. In the case of a density dependence equivalent to a 3-body interaction, the Hamiltonians kernel can be expressed in terms of the left right mixed density [21]:

$$\rho(\mathbf{r}) = \sum_{\mu\nu\sigma} \langle \mathbf{a}^{+}\mathbf{b} \rangle_{\mu\nu} \Phi^{*}_{l,\mu}(\mathbf{r},\sigma)\Phi_{r,\nu}(\mathbf{r},\sigma) \tag{52}$$

We have chosen the same dependence on the mixed density when there is no equivalence with a three-body interaction. The energy is then expressed as a functional of $|R\rangle$ and $|L\rangle$ similar to the mean-field functional. One can show that the mixed density depends only on the relative angles between the principal axes of $|R\rangle$ and $|L\rangle$. Therefore, after integration on the Euler angles, the energy is real and does not depend on the orientation of the reference frame. One can thus restore symmetries either on the left or the right wave function.

3 Application to ^{24}Mg

The results shown in this section have been obtained using the HF+BCS wave functions generated with an axial quadrupole constraint. The Lipkin-Nogami prescription has been used to improve the treatment of pairing correlations. It has indeed been shown that this prescription permits to generate wave functions which are reasonable approximations of those obtained by a variation after projection on the good particle number [27]. In this way, the lack of a complete variation after projection should be partly compensated. The mean-field results that we will present below correspond to these HF+BCS+LN calculations.

Since our aim is mainly to test the properties of our method, we have performed calculations with three Skyrme parameterizations which have given satisfactory results in the description of rotational bands in well deformed nuclei, namely SIII [28], SkM* [29], and SLy4 [30]. The pairing interaction is a zero range interaction similar to the ones used in previous studies of super-deformed bands [2], and of nuclei far from stability [31]. In calculations performed with SLy4, we have varied the strength of the density-dependent pairing force from $G = 1250 MeV fm^3$ to $G = 900 MeV fm^3$. Most results did not depend significantly on the value of G, the most sensitive quantity being the excitation energy of the first 2^+ state. We have chosen to show here only results obtained with $G = 1000 MeV fm^3$ which gives a 2^+ energy close to experiment. The same value of the pairing strength has been used for the two other Skyrme parametrizations. It is clear that a precise adjustment of the pairing strength requires a study of a large range of isotopes, a work which is in progress. We have also tested the density independent zero-range pairing interaction that has been adjusted for a study of super-heavy nuclei [32].

In figure 1 are shown the mean-field energies as a function of prolate deformations with the three Skyrme interactions and, in the case of SLy4, of a surface and a volume pairing force (dashed curves). Since oblate deformations play a minor role in this nucleus, they have not been represented. The curves are similar, with a well deformed prolate minimum corresponding to a mass quadrupole moment of approximately 1 b. The curvature is slightly different in the four cases, the volume pairing leading to the deepest minimum.

The energies obtained by projecting each of the mean-field wave functions on good particle number and angular momentum are also shown on figure 1. The abscissa of the projected energies correspond to the quadrupole moment of the intrinsic wave function. The spherical configuration is a pure 0^+ state and

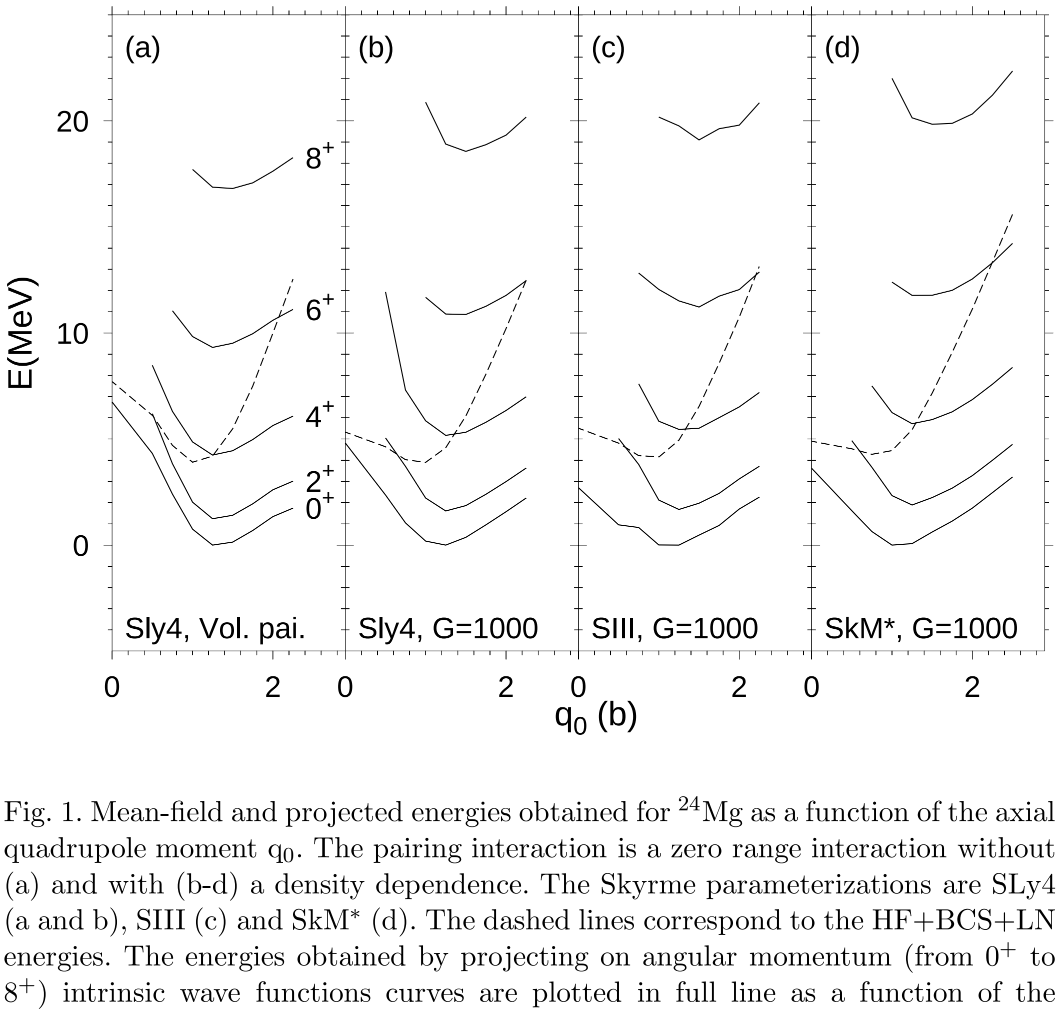

Fig. 1. Mean-field and projected energies obtained for ^{24}Mg as a function of the axial quadrupole moment q_0. The pairing interaction is a zero range interaction without (a) and with (b-d) a density dependence. The Skyrme parameterizations are SLy4 (a and b), SIII (c) and SkM* (d). The dashed lines correspond to the HF+BCS+LN energies. The energies obtained by projecting on angular momentum (from 0^+ to 8^+) intrinsic wave functions curves are plotted in full line as a function of the quadrupole moment of the intrinsic wave function.

contributes only to the 0^+ projected curve. The energy gained by projection in this case is due to the difference between the Lipkin Nogami approximation of the energy gain due to projection on particle number, $-\lambda_2 \Delta N^2$, and the exact gain. It is of the order of 1 MeV in all cases, except in the calculation with the SIII force, where it is significantly larger. This may be due to that a lower value for the pairing energy is obtained in the SIII calculation and that the LN prescription is less accurate in the low pairing regime.

In all cases, the projection on angular momentum increases the energy difference between the spherical configuration and the minimum of the J=0^+ curve by 3 to 4 MeV. The intrinsic wave function leading to the minimum of this curve has a quadrupole moment slightly larger than the one corresponding to the mean-field minimum. For higher angular momenta, the minima are shifted to higher quadrupole moments. The dependence of the curves on the nuclear interaction is rather weak for all J values other than 0; for J=0, the differences are mainly related to differences between the spherical configurations.

On figure 2, the weights of the various angular momenta in the mean-field wave functions are plotted as a function of the axial quadrupole moment. These weights do not depend significantly on the nuclear interaction; results obtained with the SLy4 force and a surface pairing are only shown.

The spherical configuration is already an eigenstate of the angular momentum operator and is affected only by the particle number projection. Its N=Z=12 component has a weight of 0.18, the remaining part corresponding to different proton and neutron numbers. The J=0 curve displays a pronounced peak around the spherical point. It is not symmetric with respect to quadrupole moment, the weights on the prolate side being larger than on the oblate side. For this reason, the J=0 curve is rather far from a Gaussian. This shows that the Gaussian overlap approximation sometimes used to derive a collective Shrodinger equation should be used with care. When the weight of a mean-field wave function component is lower than 0.01, the projection becomes numerically difficult; such tiny components have been excluded from the configuration mixing calculations. As expected, the quadrupole moment correspondig to the largest weight moves to higher quadrupole moments as a function of angular momentum. For J=10^+, no maximum is obtained up to a quadrupole moment of 4.5 b, showing that our variational space is inadequate to describe accurately states with such a high spin. A dissymetry between the prolate and oblate deformations can also be noticed on figure 2: the total weights corresponding to N=Z=12 are twice larger for prolate configurations than for oblate ones. This confirms that ^{24}Mg is dominated by prolate configurations. The different dispersions in particle numbers for prolate and oblate deformations is at the origin of this dissymetry (upper part of the figure).

The variation of the energy as a function of prolate and oblate deformations is

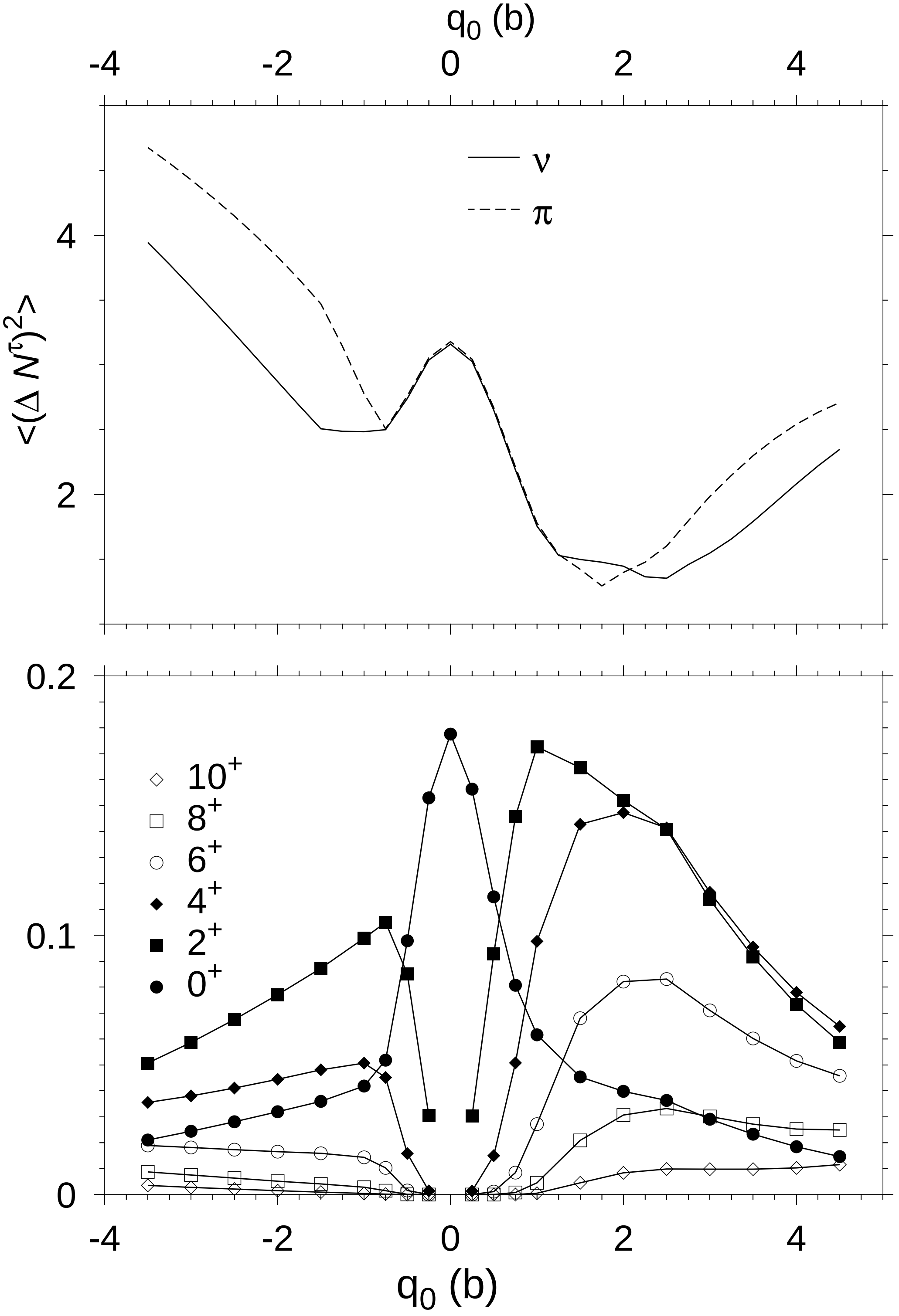

Fig. 2. Lower part: weights $\langle \Psi^{N_0,Z_0}_{J_0,M=0} | \Phi(q_0) \rangle$ as a function of q$_0$ and J calculated in case (b) of fig. 1. Upper part: particle number dispersions in the intrinsic wave functions as a function of q_0 for neutrons (full line) and for protons (dashed line).

plotted on figure 3 for the SLy4 Skyrme parametrization and a surface pairing interaction. In addition to the prolate minimum already observed on figure 1, the mean-field curve presents a shoulder at an oblate deformation around 0.5 b. The full projection creates an oblate minimum at the position of that shoulder for J values ranging from 0^+ to 6^+. For greater values of J, the weights of the intrinsic wave functions for deformations below -2 b are very small. Consequently, the projected energy curves do not exhibit any oblate minima. However the J=0^+ to 6^+ minima are probably not stable against triaxial deformations, since a calculation including triaxial deformations indicates that

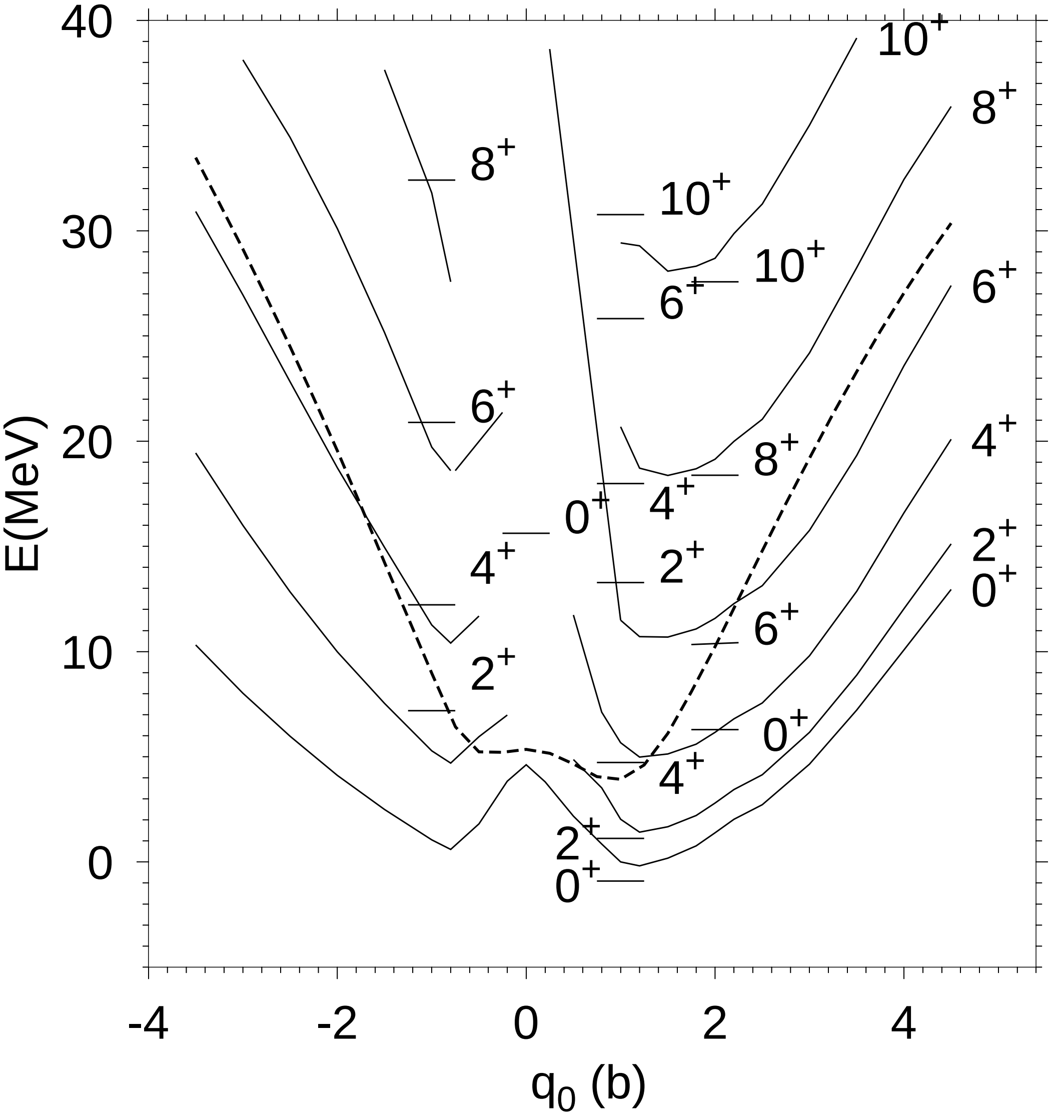

Fig. 3. Projected energies for ^{24}Mg as a function of the axial quadrupole moment (case (b) of fig. 1). The symbols are the same as in the previous figures. The first three energies obtained for each angular momentum in the configuration mixing calculation are represented by horizontal bars centered at the value of q_0 where the respective collective wave functions are maximum.

the shoulder in the intrinsic curve is a maximum with respect to γ.

For each value of the angular momentum, we have performed a configuration mixing calculation including quadrupole moments between –3.5 b and 4.5 b. This corresponds to intrinsic configurations excited by about 30 MeV with respect to the prolate minimum. This configuration mixing is nothing but a variation after projection in a limited but hopefully relevant Hilbert space. The spectrum generated in this way (represented by bars) is plotted at the quadrupole moment corresponding to the largest component of the collective

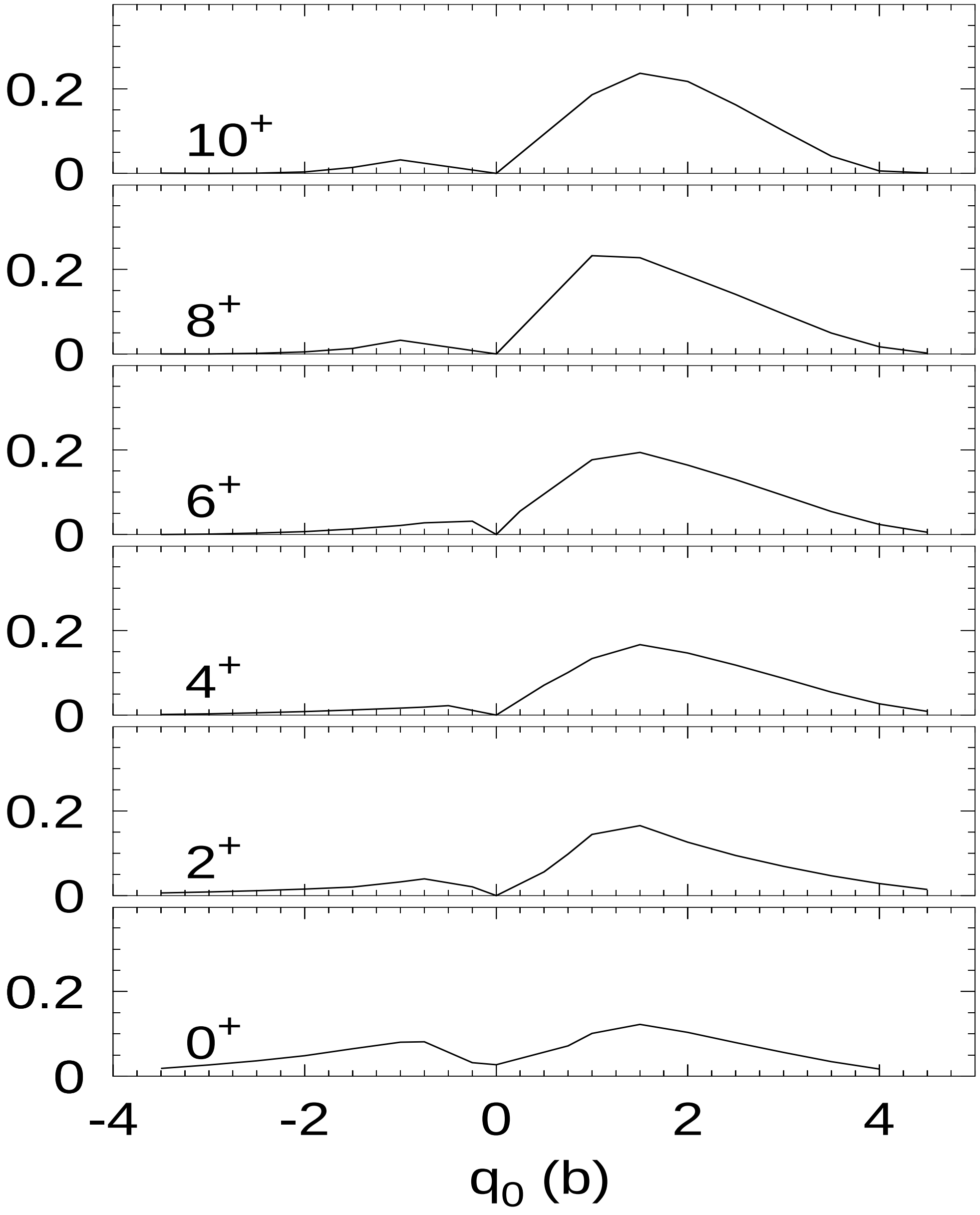

Fig. 4. Squared weights of intrinsic states in the Yrast levels ($l = 0$) of the different angular momentum representations.

wave function, which are shown on figure 4 for the yrast states. The value of this quadrupole moment is very close to the minimum of the projected energy curve. Moreover, the energy of this minimum is slightly modified by the configuration mixing. The largest gain, ~800 keV, is obtained for the 0^+ state, but is reduced at higher spins. Several excited states are found at low energy for each spin value. Except for the second 0^+ and 10^+, the wave functions of yrare states are peaked around the oblate secondary minimum.

The spectra obtained with the four choices of interactions described for fig. 1 are compared to the experimental spectrum [33] on figure 5. The energies correspond to the minima of the projected energy curves except in the column (b') where the configuration mixing spectrum is represented. For comparison, we show also the results of a cranking calculation performed with the SLy4 interaction and a surface pairing with the same strength of 1250MeV that we used in our calculations of SD rotational bands. In this case, we use the HFB+Lipkin-Nogami method presented in our previous cranking calculations [2].

Since the intrinsic ground state of ^{24}Mg has a large prolate deformation, one expects the cranking approximation to be valid. The cranking spectrum is indeed in good agreement with the experimental data up to the 6^+ level. Ex-

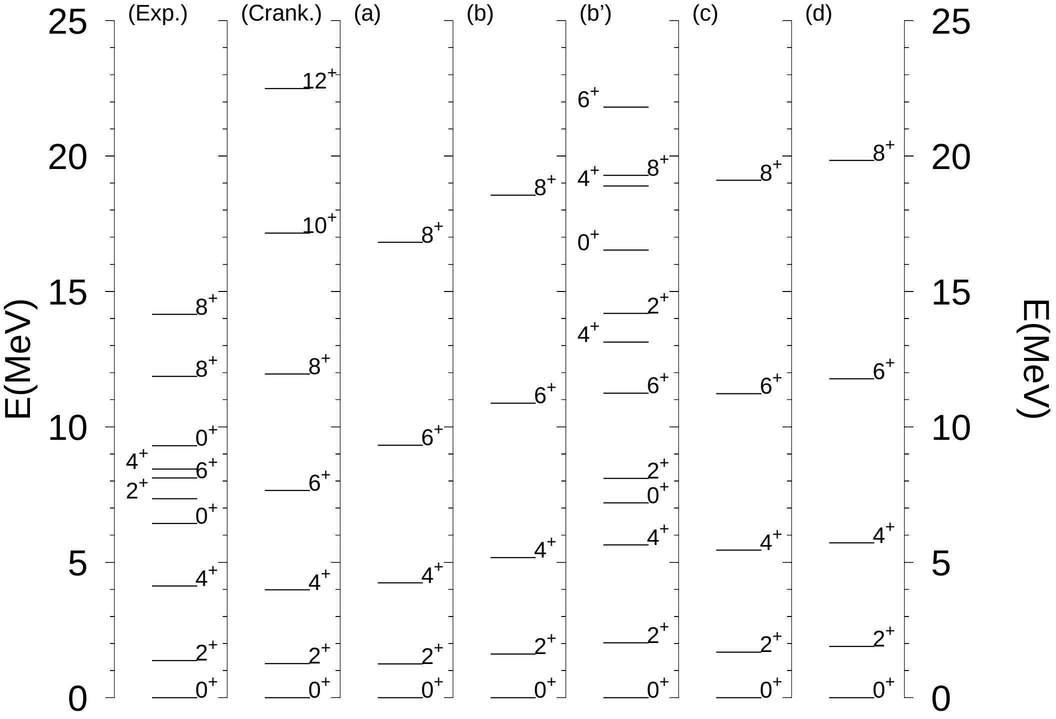

Fig. 5. Experimental positive parity levels of ^{24}Mg compared to a cranking calculation (SLy4 and density-dependent zero-range pairing interactions) and to the (a)-(d) choices of interactions described in fig.1. In the column (b') is plotted the configuration mixing spectrum.

perimentally, it is the second 8^+ which belongs to the ground state rotational band and our result underestimates its energy by 2.0 MeV. The energy at which we obtain a 10^+ state is probably also too low. In the cranking calculation, the pairing energy becomes very small at spin 8; triaxiality effects become also important around this spin.

In the projected spectra, the energy of the first 2^+ state is systematically overestimated, the energy obtained with a volume dependent pairing being however rather close to the experimental value. Two restrictions imposed in the present calculation may be at the origin of this discrepancy. First, we have not included triaxial deformations, which are shown by the cranking calculation to be more important at high spins than at low spins. Second, the variation after projection on angular momentum is limited to the quadrupole moment; the mean-field equations are optimized for the description of the ground state energy and not for excited states. The first limitation could be removed with minor modifications of the formulae presented in section 2. However, the computing time would be largely increased, the number of Euler angles for the angular integration being at least 50 times larger. A rather simple way to improve the variational character of the calculation would be to project for each spin wave functions generated by cranking calculations. It is indeed well known [8] that cranking is a first order approximation of a variation after projection on angular momentum. To generalize our method in this direction requires mainly to consider Bogoliubov instead of BCS transformations, a fact which would not increase too much the computing time. Work along this line is in progress.

One of the main interests of a restoration of rotational symmetry is the possibility to calculate transition probabilities without the approximation involved in a cranking calculation. On figure 6, are compared to the experimental data [33] the transition probabilities along the yrast line obtained in the GCM calculation and by considering only the minima of projected energy curves. The value of the 2^+ to 0^+ B(E2) is nearly independent of the nuclear interaction and results are only shown for the SLy4 interaction (case b). The transition probability between the configurations minimizing the projected energy curves is very close to the experimental value. The configuration mixing causes a spreading of the collective wave function on the quadrupole moment and decreases slightly the value of the B(E2). This effect is similar to the effect of quadrupole vibrations that is sometimes included phenomenologically [11] in the determination of transition probabilities from intrinsic wave functions. Since for spin different from 0, the wave functions do not have components at low quadrupole moment, the configuration mixing does not affect significantly the transition probabilities. The agreement between both calculations and the experimental data is excellent in these cases.

In our first studies of quadrupole collective dynamics [34], we have introduced an approximate projection on 0^+ and 2^+ states from intrinsic states. This projection is based on the mixing of the configurations corresponding to all the possible labellings of the principal axes of inertia. It is supposed to be valid for small deformations. The present calculation gives the opportunity to test the validity of this approximate projection. On figure 7 are plotted the energy curves corresponding to the mean-field calculation, projection on particle number only, projection on particle number together with mixing of the three possible orientations of the principal axes and triple projection. The effect of particle number projection is dominant for small deformations, corresponding to a β value up to 0.1. The restricted projection on angular momentum gives a fair approximation for slightly larger deformations, up to β

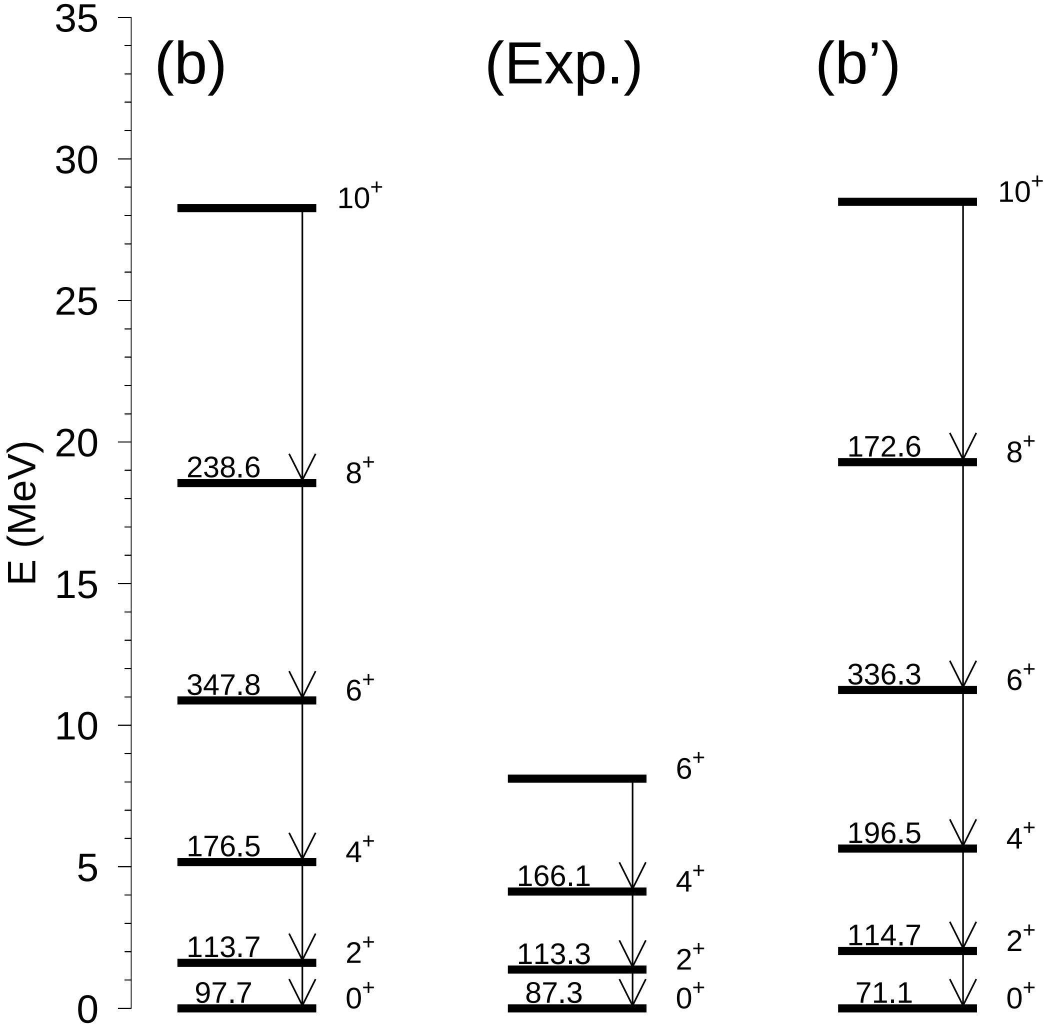

Fig. 6. $B(E2)$ transition probabilities (in $e^2 fm^4$ for ^{24}Mg. Transition probabilities between the configurations corresponding to the minimum of the projected energy curves of figure 3 (left side) and between the yrast collective states obtained in the GCM calculation (right side). In the central part are shown the experimental values [33].

around 0.2. For still larger quadrupole moments, the full projection becomes necessary. On the right part of the figure are compared the configuration mixing spectra obtained with the exact and the approximate projections. The differences in total energy are due to the failure of the approximate projection above quadrupole moments of 0.5 b. However, the relative position of the first 0^+ and 2^+ is rather satisfactorily estimated.

The restricted projection is of limited interest for a well deformed nucleus like ^{24}Mg. However for heavy spherical nuclei, its validity up to a β value around 0.2 makes it a cheap alternative to study quadrupole dynamics.

4 Conclusion

In this paper, we have presented and tested a method to introduce correlations beyond mean-field on HF+BCS wave functions. The formulae given in the first

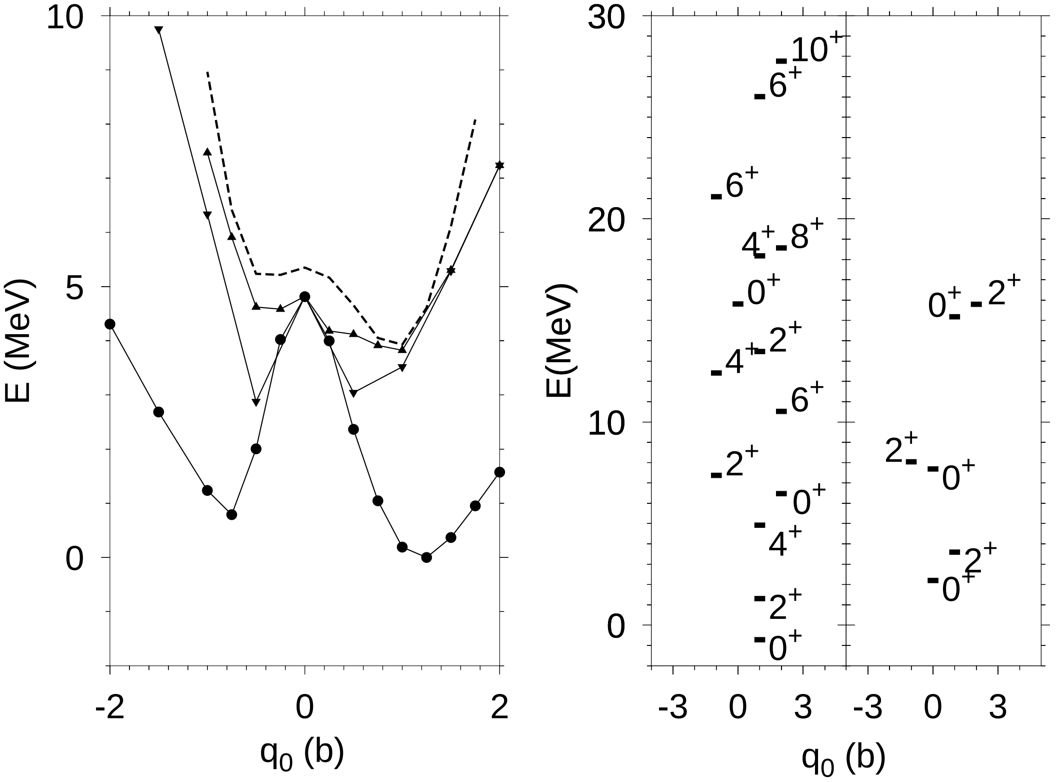

Fig. 7. On the left part of the figure are shown the energy curves corresponding to the mean-field calculation (dashed line), projection on particle number only (up triangles), projection on particle number together with mixing of the three possible orientations of the principal axes (down triangles) and triple projection (dots). On the right are compared the configuration mixing energies obtained with the full (on the left) and the restricted (on the right) projections.

part of section 2 are written in a form appropriate for the relaxation of the restrictions imposed in this study. The extensive tests performed on the ^{24}Mg nucleus show that the method works with reasonable computing time.

A first and natural generalization from BCS to full Bogoliubov-Valatin transformations is under progress. It will allow a better treatment for pairing correlations. If no significant improvements for even-even nuclei close to the stability line is to be expected, HFB is essential to treat correctly nuclei near the drip lines (see ref. [31,35]).

As the projection onto angular momentum implies that one cannot anymore make use of the signature symmetry, the generalization to many-body wave functions breaking time reversal invariance is a natural next step. That is a necessary step towards a description of odd nuclei. It will also enable to project wave functions generated for each spin by cranking calculations. As it has already been shown theoretically [7,8], the use of cranking wave functions is the first order of a variation after projection on angular momentum. Numerical applications [15,25] have confirmed that the projection of cranking wave functions improves the energy obtained for each angular momentum and compresses the spectra. Such an effect would correct the too spread spectra obtained in the present study.

Another important question for which we have preliminary answers concerns the use of effective interactions adjusted for mean-field calculations in a model where are incorporated correlations beyond HF+BCS. The Skyrme parametrizations that we have tested here behave in a similar way and are reasonable starting points to study the effects of correlations. We have started a study of several Mg isotopes and of a few neighbouring nuclei is underway. This should enable to better determine the properties of effective interactions on which depend the spectra of nuclei far from stability.

5 Acknowledgements

This research was supported in part by the PAI-P3-043 of the Belgian Office for Scientific Policy.

References

[1] B. Gall, P. Bonche, J. Dobaczewski, H. Flocard and P.-H. Heenen, Z. Phys. **A348** (1994) 183.

[2] J. Terasaki, P-H Heenen, P. Bonche, J. Dobaczewski and H. Flocard, Nucl Phys **A593** (1995) 1.

[3] C. Rigollet, P. Bonche, H. Flocard and P.-H. Heenen, Phys. Rev. **C59** (1999) 3120.

[4] A. Valor, J.L. Egido, L.M. Robledo, Phys. Lett. **B392** (1997) 249.

[5] A. Valor, J.L. Egido and L.M. Robledo, preprint (1999).

[6] S. Islam, H.J. Mang and P. Ring, Nucl. Phys. **A326** (1979) 161.

[7] H.J. Mang, Phys. Rep. **18C** (1975) 327.

[8] P.Ring and P. Schuck, *The Nuclear Many Body Problem*, Springer Verlag, Berlin, 1980.

[9] X. Campi, H. Flocard, A.K. Kerman and S. Koonin, Nucl. Phys. **A251** (1975) 193.

[10] M. Girod and B. Grammaticos, Nucl. Phys. **A350** (1979) 40.

[11] P.G. Reinhard, D.J. Dean, W. Nazarewicz, J. Dobaczewski, J.A. Maruhn and M.R. Strayer, Phys. Rev. **C60** (1999)

[12] K. Hara and Y. Sun, Int. J. Mod. Phys. **E4** (1995) 637.

[13] K. Enami, K. Tanabe and N. Yoshinaga Phys. Rev. **C59** (1999) 135.

[14] E. Caurier and B. Grammaticos, Nucl. Phys. **A279** (1977) 333.

[15] D. Baye and P.-H. Heenen Phys. Rev. **C29** (1984) 1056.

[16] R. Rodríguez-Guzmán, J.L. Egido and L.M. Robledo, (1999) preprint.

[17] P.-H. Heenen, P. Bonche, J. Dobaczewski and H. Flocard, Nucl. Phys. **A561** (1993) 367.

[18] J.L. Egido, L.M. Robledo and Y. Sun, Nucl. Phys. **A560** (1993) 253.

[19] D.L. Hill and J.A. Wheeler, Phys. Rev. **89** (1953) 1102.

[20] R. Balian and E. Brézin, Il Nuovo Cimento, Vol. LXIV B, (1969) 37.

[21] P. Bonche, J. Dobaczewski, H. Flocard, P.-H. Heenen and J. Meyer, Nucl. Phys. **A510** (1990) 466.

[22] P. Bonche, H. Flocard and P.-H. Heenen, Nucl. Phys. **A467** (1987) 115.

[23] D. Baye and P.-H. Heenen, J. Phys. A : **19** (1986) 2041.

[24] H. Flocard, Ph.D. Thesis (1975), unpublished.

[25] K. Hara, A. Hayashi and P. Ring, Nucl. Phys. **A385** (1982) 14.

[26] C. W. Wong, Phys. Rep. **15C** (1975) 285.

[27] P. Magierski, S. Ćwiok, J. Dobaczewski and W. Nazarewicz, Phys. Rev. **C48** (1993) 1686.

[28] M. Beiner, H. Flocard, Nguyen Van Giai and P. Quentin, Nucl. Phys. **A238** (1975) 29.

[29] J. Bartel, P. Quentin, M. Brack, C. Guet and H.-B. Håkansson, Nucl. Phys. A386 (1982) 79.

[30] E. Chabanat, P. Bonche, P. Haensel, J. Meyer and R. Schaeffer, Nucl. Phys. **A635** (1998) 231.

[31] J. Terasaki, P.-H. Heenen, H. Flocard and P. Bonche Nucl. Phys. **A600** (1996) 371.

[32] S. Ćwiok, J. Dobaczewski, P.-H. Heenen, P. Magierski and W. Nazarewicz, Nucl. Phys. **A611** (1996) 211.

[33] D.M. Pringle, W.J. Vermeer, W.N. Catford and I.F. Wright, Conf. on Nuclear Structure, Reactions and Symmetries, Eds R.A.Mayer and V. Paar (World Scientific) Vol. 2 (1986) 632,

P.M. Endt, Nucl. Phys. **A521** (1990) 1.

[34] P. Bonche, J. Dobaczewski, H. Flocard and P.-H. Heenen Nucl Phys **A530** (1991) 149.

[35] J. Dobaczewski, H. Flocard and J. Treiner, Nucl. Phys. **A422** (1984) 103.